N-Terminal Stathmin-like Peptides Bind Tubulin and Impede Microtubule Assembly†

Marie-Jeanne Clément,[‡,§] Isabelle Jourdain,[§,||] Sylvie Lachkar,[||] Philippe Savarin,[‡] Benoît Gigant,[⊥] Marcel Knossow,[⊥] Flavio Toma,[‡] André Sobel,[||] and Patrick A. Curmi*[,‡]

Laboratoire Structure et Reconnaissance des Biomolécules, EA3637, Université Evry-Val d'Essonne, Evry, F-91025 France, INSERM, U706, Institut du Fer à Moulin, Paris, F-75005 France, UPMC, Paris, F-75005 France, and CNRS, UPR 9063, Laboratoire d'Enzymologie et Biochimie Structurales, Gif-sur-Yvette Cedex, F-91198 France

Received June 29, 2005; Revised Manuscript Received September 5, 2005

ABSTRACT: Microtubules are major cytoskeletal components involved in numerous cellular functions such as mitosis, cell motility, or intracellular traffic. These cylindrical polymers of $\alpha\beta$-tubulin assemble in a closely regulated dynamic manner. We have shown that the stathmin family proteins sequester tubulin in a nonpolymerizable ternary complex, through their stathmin-like domains (SLD) and thus contribute to the regulation of microtubule dynamics. We demonstrate here that short peptides derived from the N-terminal part of SLDs impede tubulin polymerization with various efficiencies and that phosphorylation of the most potent of these peptides reduces its efficiency as in full-length stathmin. To understand the mechanism of action of these peptides, we undertook a NMR-based structural analysis of the peptide−tubulin interaction with the most efficient peptide (I19L). Our results show that, while disordered when free in solution, I19L folds into a β-hairpin upon binding to tubulin. We further identified, by means of saturation transfer difference NMR, hydrophobic residues located on the β2-strand of I19L that are involved in its tubulin binding. These structural data were used together with tubulin atomic coordinates from the tubulin/RB3−SLD crystal structure to model the I19L/tubulin interaction. The model agrees with I19L acting through an autonomous tubulin capping capability to impede tubulin polymerization and provides information to help understand the variation of efficiency against tubulin polymerization among the peptides tested. Altogether these results enlighten the mechanism of tubulin sequestration by SLDs, while they pave the way for the development of protein-based compounds aimed at interfering with tubulin polymerization.

Microtubules are prominent components of the cytoskeleton required for the dynamic organization of the intracellular space. They contribute to the traffic of intracellular cargos and organelles and, in dividing cells, participate in the formation and the segregating activity of the mitotic spindle. Microtubules are highly dynamic polarized cylinders of polymeric $\alpha\beta$-tubulin protofilaments involved in the rapid and constant remodeling of the cytoskeleton in response to the cell needs. The intrinsic dynamicity of microtubules is regulated in the cell by numerous proteins binding either to assembled microtubules or, like stathmin and stathmin family proteins, to the free $\alpha\beta$-tubulin heterodimer in solution.

Stathmin (*1*) is a ubiquitous cytosolic phosphoprotein proposed to integrate diverse intracellular signaling pathways (*2*) that may interfere with various microtubule-dependent cell functions (*3*, *4*). Stathmin controls microtubule assembly by sequestering tubulin in a nonpolymerizable ternary complex made of two $\alpha\beta$-tubulin heterodimers for one stathmin molecule (T_2S complex), whose stability is decreased by stathmin phosphorylation (*5*−*11*). Alternatively, it has been proposed that stathmin directly favors microtubule catastrophes (*4*, *11*, *12*), although this property is not documented as the sequestration activity. Finally, stathmin is the generic element of a gene and protein family, including SCG10, SCLIP, and RB3 (*13*−*16*), which all sequester tubulin in a T_2S-like complex (T_2SLD) through their highly conserved stathmin-like domain (SLD) (*17*).

The recent crystallographic structure of a tubulin−colchicine/RB3−SLD complex at 3.5 Å (*18*) revealed three domains within the SLD: an N-terminal cap domain (residues 4−28), a linker domain (29−45), and a long, mostly α-helical domain (46−145) bearing two duplicated tubulin-binding sites. The N-terminal domain of RB3−SLD caps α-tubulin at a position and in a way that may prevent the longitudinal addition of the capped tubulin to the plus ends of growing microtubules. This observation is in agreement with earlier results showing that the presence of the N-

† This work was supported by Institut National de la Santé et de la Recherche Médicale, Association pour la Recherche sur le Cancer (ARC), Ligue Nationale Contre le Cancer. The Région Ile de France, the Conseil Général de l'Essonne, Genopole, DSV/CEA, and the Association Française de lutte contre la Myopathie (AFM) are acknowledged for their contribution to the NMR equipment. M.-J.C. is the recipient of a postdoctoral fellowship from Ligue Nationale contre le Cancer. I.J. is the recipient of a doctoral fellowship from ARC, and P.A.C. is the recipient of an ATIGE grant from Genopole.

* To whom correspondence should be adressed. Telephone: 33-(0)1-69-47-01-87. Fax: 33-(0)1-69-47-01-72. E-mail: pcurmi@univ-evry.fr.

‡ Université Evry-Val d'Essonne.

§ These authors contributed equally to this work.

|| INSERM and UPMC.

⊥ CNRS.

10.1021/bi0512492 CCC: $30.25
Published on Web 10/14/2005

terminal region of stathmin prevents the longitudinal assembly of T_2S complexes into rings (*7*). Accordingly, cross-linking experiments demonstrated an interaction between the N terminus of stathmin with helix 10 of α-tubulin (*19*), a critical secondary structure element involved in the establishment of longitudinal protofilament contacts (*20*). Overall, this capping property of stathmin and SLDs has been proposed, in addition to the stabilization of tubulin in a curved conformation, as one of the mechanisms accounting for their tubulin sequestering ability (*7*, *18*, *19*, *21*). A closer view of the N-terminal cap domain of RB3−SLD in the tubulin−colchicine/RB3−SLD complex shows the presence of a *β*-hairpin motif that possesses residues in an interaction with some of the α-tubulin residues involved in the inter-dimer longitudinal contacts when assembled in protofilaments (*18*). The presence of such a defined fold and the good conservation of the N-terminal region in the stathmin family prompted us to check whether isolated short peptides from this region might represent a minimal functional unit able by itself to impede tubulin polymerization.

In the present study, we demonstrate that such peptides derived from stathmin family proteins function as potent autonomous inhibitors of tubulin assembly. The NMR structural study of I19L, the most efficient of these peptides, revealed that, while the free peptide has no preferred conformation, it adopts in solution a *β*-hairpin structure upon interaction with tubulin, close to that observed in tubulin−SLD crystals by X-ray analysis. Saturation transfer difference NMR (STD−NMR) spectroscopy (*22*) allowed us to identify side chains of residues of I19L in contact with tubulin. This information, combined with docking computations, highlight essential features of the interaction of the I19L peptide with tubulin and open perspectives for designing novel tubulin/microtubule-interfering agents.

MATERIALS AND METHODS

Bovine Brain Tubulin Preparation. Tubulin was purified from bovine brain crude extracts by three cycles of polymerization (*23*), followed by phosphocellulose chromatography (*24*). It was stored at −80 °C in 50 mM Mes-KOH, 0.5 mM dithiothreitol, 0.5 mM EGTA, 0.25 mM $MgCl_2$, 0.5 mM EDTA, 3.4 M glycerol, and 0.1 M GTP at pH 6.8 for long-term storage. Before use, an additional cycle of polymerization was performed, at the end of which tubulin was resuspended in 12.5 mM Mes-KOH, 0.25 mM EGTA, and 0.25 mM $MgCl_2$ at pH 6.8. The tubulin concentration was determined by spectrophotometry using an extinction coefficient of 1.2 mg^{-1} cm^2 at 278 nm (*25*).

Peptides. Peptides were obtained from Epytop (Nimes, France). The peptide synthesis was done using Fmoc [*N*-(9-fluorenyl)methoxycarbonyl] chemistry, and the purity and integrity of the peptides were verified by mass spectroscopy. The peptides were dissolved in water and if necessary solubilized with NH_4OH.

In Vitro Tubulin Polymerization Assay. Tubulin polymerization was monitored turbidimetrically at 350 nm in an Ultrospec 3000 spectrophotometer (Pharmacia Biotech) thermostated at 37 °C (1 cm light path). Experiments were carried out in 50 mM MES-KOH at pH 6.8, 30% glycerol, 0.5 mM EGTA, 6 mM $MgCl_2$, and 0.5 mM GTP (buffer M). Tubulin polymerization in each sample was evaluated by the difference between the 37 °C steady-state absorbance and the absorbance reached after subsequent 15 min cold-induced depolymerization at 0 °C, which allows us to ensure that the absorbance at 350 nm taken into account indeed results from polymerized tubulin and not from cold stable aggregates (*5*). The difference between the two values were used to construct critical concentration plots representing the amount of polymerized tubulin observed at steady state versus the total concentration of tubulin, measured in the absence or presence of peptides, as described (*17*). The normalized steady-state OD_{350} were measured for a solution containing 20 μM tubulin in the presence of increasing concentrations of peptides. Normalized OD_{350} was calculated as follows:

$$\text{normalized } OD_{350} = \text{steady-state } OD_{350} / \text{steady-state } OD_{350} \text{ for 20 } \mu\text{M tubulin alone}$$

IC_{50} values (concentration of the peptide that inhibits tubulin polymerization to 50% of the control value) were obtained from curves shown in Figure 2 using a linear data fitting program.

Circular Dichroism (CD). The far-UV CD spectra were recorded on a Jasco 700 spectropolarimeter in a 0.1 cm quartz cell. The spectra were obtained as an average of four runs and were corrected for the contribution of the buffer. Experiments were repeated twice, and the data were averaged to reduce noise. The scan speed was 5 nm/min. Protein concentration was 50 μM.

NMR Spectroscopy. All ^{1}H NMR experiments were performed at 294 K on a Bruker Avance 600 MHz NMR spectrometer equipped with a cryoprobe, and data were processed using XWINNMR (Bruker) software. Sodium [3-trimethylsilyl 2,2′,3,3′-2H4] propionate (TSP-d4) was used as an internal reference for proton chemical shifts.

Spectra of free I19L were collected on a 0.6 mM peptide sample in a mixture of H_2O:D_2O (90:10) pH 6.8 and in 60% CD_3OH. The NMR sample of I19L in the interaction with tubulin contained 0.6 mM of peptide and 20 μM of tubulin, for a ratio of 30:1 peptide:protein, in a 50 mM sodium phosphate buffer at pH 6.8, containing 0.02% NaN_3 and 10% D_2O. A control sample was prepared the same way with I19L and bovine serum albumin (BSA) to detect nonspecific interactions. One-dimensional proton spectra were acquired with 64 scans and 16 K data points. For sequence-specific assignments, two-dimensional DQF−COSY (*26*), TOCSY (*27*), NOESY (*28*), and ROESY (*29*) spectra were used. The TOCSY experiments were acquired using the MLEV17 sequence (*30*) with a mixing time of 100 ms. In the NOESY and TRNOESY (*31*, *32*) experiments, the mixing period was 200 ms. Two-dimensional ROESY spectrum was recorded with a mixing time of 300 ms. All two-dimensional experiments were carried out with 2048 data points × 512 increments × 64 scans and a spectral width of 6000 Hz in both dimensions. The data were zero-filled to give 4096 × 1024 data matrix prior to Fourier transformation. One-dimensional STD−NMR experiments (*22*) of I19L in the interaction with tubulin were recorded with 1024 scans. The protein resonances were saturated at 0 or 10 ppm (40 ppm for reference spectra) with a cascade of 40 selective Gaussian-shaped pulses of 50 ms duration, with a 1 ms delay between each pulse, resulting in a total saturation time of

2.04 s. Subtraction of saturated spectra from reference spectra was performed by phase cycling. For 2D STD−TOCSY spectra, two experiments were collected with selective saturation at 0 and 40 ppm, respectively, and the spectra were then subtracted. They were recorded with 2048 data points × 256 increments × 32 scans. In all experiments, suppression of the water signal was achieved with the WATERGATE sequence before acquisition (*33*). The NMR spectra were visualized and analyzed with NMRView 5.0.4. (*34*).

Structure Calculations. Distance constraints for structure calculations were derived from the 200 ms mixing time TRNOESY spectrum. The volume of the NOESY cross-peaks was measured with NMRView and converted to distances using the relationship $I_{ij}/I_{ref} = ((r_{ref}/r_{ij})^6)$ (*35*) using the distance between the Phe-20 Hβ protons (1.74 Å) as a reference. An error of ±10% was applied for all distances. A total of 200 structures were calculated with CNS 1.1 (*36*) using a standard simulated annealing protocol. Of these calculated structures, the quality of the 20 structures with lower total energy was analyzed with PROCHECK 3.5.4 (*37*), and the 10 best structures being most consistent with the experimental data were selected and visualized with MOLMOL 2.6 (*38*).

Docking Procedure. I19L and tubulin were docked together with FTDOCK (*39*), a rigid docking protocol based on shape and electrostatic complementarities. The average calculated structure of I19L and the tubulin crystal structure of tubulin−colchicine/RB3−SLD complex (PDB 1SA0) were used for the docking calculations. The multiple predictions (10 000) generated were then filtered using our STD−NMR data and X-ray crystallographic data (*18*). Thus, we excluded first all predictions that resulted in a distance larger than 4.5 Å between side chains of Ala-19, Phe-20, Leu-22, and Leu-24 of I19L and α-tubulin; then, among the remaining predictions, only those that had a distance less than 4.5 Å between residues of the α-tubulin interdimer interface and I19L residues were kept for further analyses. Finally, the complex with the best shape and electrostatic complementarities was selected and submitted to 50 cycles of unrestrained Powell minimization using CNS 1.1.

RESULTS

Peptides Derived from the Capping N-Terminal Sequence of SLDs Inhibit Tubulin Polymerization with Various Efficiencies. We first tested the hypothesis that peptides from the N-terminal part of the various SLDs may be able to bind and impede tubulin polymerization by themselves, independently from their participation in the formation and stability of a T_2/SLD complex. We designed a series of synthetic peptides (Figure 1) on the basis of the capping β-hairpin region observed in the tubulin−colchicine/RB3−SLD crystal: (i) "long" peptides, covering slightly more than the corresponding β-hairpin region, from stathmin, SCG10, SCLIP, or RB3 (I19L, D26P, G26D, and M19L, respectively), (ii) two additional, "short" stathmin and RB3 peptides (Y14N and S13S, respectively), corresponding approximately to the β-hairpin strand facing α-tubulin, and (iii) finally, a version of I19L (I19L-P), phosphorylated on serine 16, an *in vivo* phosphorylation site of stathmin by different kinases such as PKA (*40*), CaMK II (*41*), CaMK IV/Gr (*42*), or PAK1 (*43*).

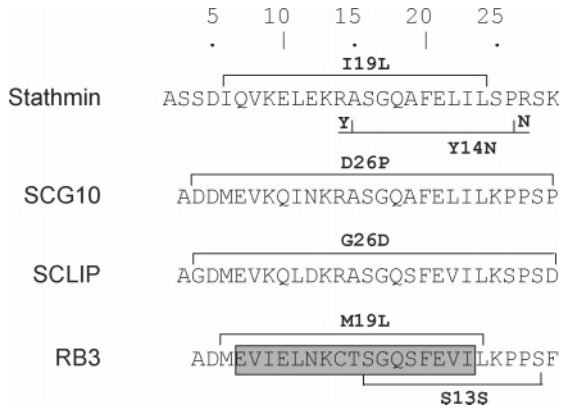

FIGURE 1: Long and short peptides from N-terminal regions of human SLDs encompass the region that forms a β-hairpin in the tubulin−colchicine:RB3−SLD crystal (boxed in gray) or the β-strand that faces tubulin (Y14N and S13S), respectively. The nomenclature of peptides is as follows: first and last letters correspond to first and last amino acid residues, and number corresponds to the number of residues. Y14N is a peptide that was used previously for immunological purposes (*54*) and therefore contains two substitutions at its first and last residues. (Stathmin numbering).

The effects of these peptides on tubulin assembly were evaluated by *in vitro* tubulin polymerization assays. When added at increasing concentrations to a solution containing 20 μM tubulin, all of the "long" peptides inhibited tubulin polymerization (Figure 2). The various peptides displayed however different efficiencies, with IC_{50} values from 65 to 425 μM (Figure 2). The most potent of them is the 19-residue-long stathmin peptide (I19L), which, under our experimental conditions, totally prevented microtubule assembly at a concentration of ∼130 μM. The less efficient of the series was the RB3 peptide (M19L), for which a 6.5-fold higher concentration was required to fully inhibit microtubule formation under the same experimental conditions. A linear relationship was observed between the peptide concentration and inhibition of tubulin polymerization for all peptides. This result suggests that the inhibition is due to a direct, stoichiometric interaction of the peptides with tubulin to form a tubulin/peptide complex that prevents longitudinal interactions among tubulin heterodimers, rather than binding to assembled microtubules, for example, with α-subunits accessible at their minus ends. Interestingly, the "short" peptides covered half of the β-hairpin region that, corresponding to stathmin (Y14N), still displayed some tubulin polymerization inhibitory activity, although it was about 27 times less efficient than its "long" counterpart, whereas the "short" RB3 peptide (S13S) produced no detectable inhibition. Finally, the phosphorylated I19L stathmin peptide interfered with tubulin assembly less efficiently than its nonphosphorylated counterpart, with a 4-fold inhibition decrease (Figure 2).

Solution Structure of the Stathmin I19L Peptide. The results described above provide evidence that peptides derived from the N-terminal "capping" domain of SLDs directly and autonomously participate in the inhibition of tubulin polymerization. To better understand the molecular mechanism of this effect and the reasons for the observed differences of efficiency among the various peptides, we examined by NMR and molecular modeling the free and tubulin-bound solution structures of the most potent peptide from our series, the I19L stathmin peptide.

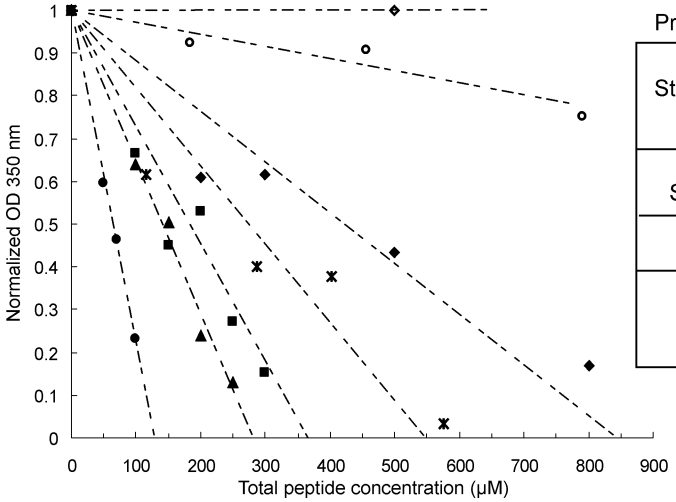

Protein	Peptide	IC50 (μM)
Stathmin	● I19L	65
	✱ I19L-P	280
	○ Y14N	1760
SCG10	■ D26P	185
SCLIP	▲ G26D	140
RB3	◆ M19L	425
	◇ S13S	ND

FIGURE 2: Peptides from N-terminal regions of human SLDs inhibit tubulin polymerization. Pure tubulin (20 μM) was left to polymerize into microtubules in M buffer at 37 °C in the presence of a varying concentration of peptides. The normalized net steady-state $A_{350\ nm}$ turbidity (which reflects microtubule mass) is reported for each peptide. Inhibition efficiencies on tubulin polymerization decreased from I19L to M19L for the long peptides. Phosphorylation of the I19L peptide led to a moderate decrease in its activity. IC_{50} values were determined as described in the Materials and Methods. ND = not determined.

I19L Is Mostly Disordered in Solution. The NMR structure of the free I19L peptide in solution was investigated at pH 6.8 in aqueous solution. All of the proton resonances of I19L were assigned at 294 K by means of two-dimensional DQF−COSY, TOCSY, NOESY, and ROESY spectra using the Wüthrich method (*44*) (see the Supporting Information). The values of the chemical shifts of the Hα protons, which are sensitive to the presence of the secondary structure were very close to those observed for random coil structures (*45*) (Figure 3B), indicating that I19L does not adopt any predominant regular secondary structure in solution. This was confirmed by the NOESY (Figure 4) and ROESY spectra, where the few cross-peaks observed correspond essentially to intraresidue or sequential NOE connectivities. The NMR results are in agreement with CD data, which showed a high percentage of random coil in the 2.5−8.3 pH range and at temperatures from 30 to 15 °C in 50 mM phosphate at pH 6.8 (not shown). However, secondary structure predictions using AGADIR indicate that I19L has a helical propensity at residues 10−14. We thus tested this propensity using different concentrations of methanol (up to 80%) in Tris-HCl at pH 6.4. The CD spectrum changed progressively into the typical α-helix spectrum (maximum positive ellipticity at 190 nm and two minima at 208 and 222 nm), reaching the maximum negative θ_{222} value for about 60% methanol (Figure 3A). Estimates of the helical content using molar ellipticity at 222 nm yielded about 1% of the helix content in 10 mM Tris-HCl at pH 6.4 and 20% helix in 80% methanol within the same buffer, suggesting that at least four residues of the peptide tend to adopt a helical conformation. The NMR study of I19L in 60% methanol-Tris buffer at pH 6.4, corroborated both the CD data and AGADIR prediction, showing the stabilization of a short α-helix at residues 10−14 under these solvent conditions (Figure 3B).

I19L in Solution Adopts a β-Hairpin Structure when Bound to Tubulin. The conformation of I19L in the interaction with tubulin was investigated using two-dimensional transferred nuclear Overhauser effect spectroscopy (TRNOESY) (*31*, *32*). The TRNOESY spectrum of I19L in the presence of tubulin ([I19L]:[tubulin] = 30:1) showed a large number of

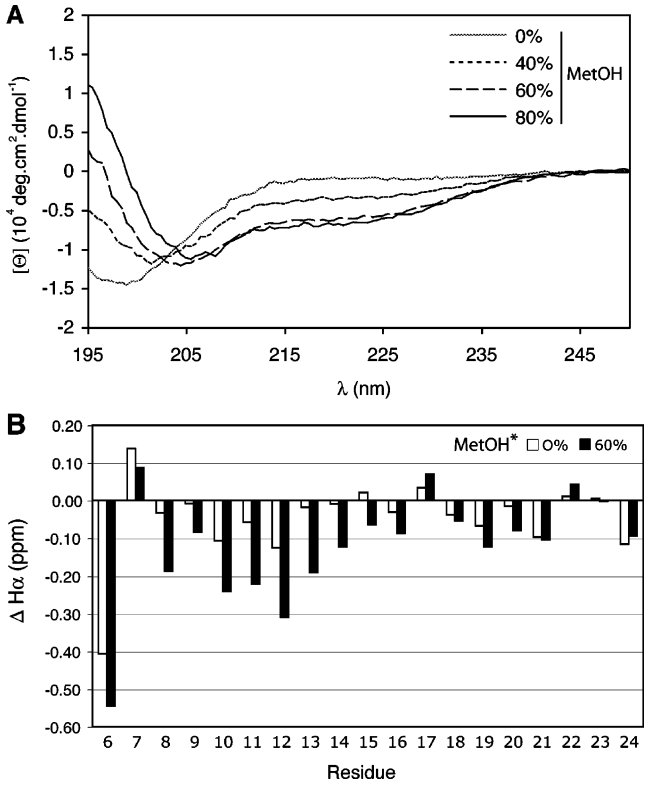

FIGURE 3: I19L has a slight α-helical propensity in the presence of methanol. (A) CD analysis of the influence of methanol on I19L folding. Far-UV spectra of 58 μM I19L recorded at 21 °C in 10 mM Tris-HCl at pH 6.4 in the presence of a varying concentration of methanol (v/v). Methanol induced 208 and 222 nm minima characteristic of the α-helical structure. (B) Differences between Hα proton chemical shifts of I19L in 90% H_2O/10% D_2O (open bars) or in 60% CD_3OH (solid bars) and random coil values (*45*). The significant negative deviations ($\Delta H\alpha < -0.1$ ppm) of Hα protons of consecutive residues 10−14 of I19L in 60% CD_3OH suggest some α-helical content. The absence of large deviations for consecutive residues of I19L in the absence of methanol (CD_3OH) implies that the peptide does not adopt a significant secondary structure.

intense negative NOEs, whereas only a few weak negative NOEs were observed in the NOESY spectrum of free I19L

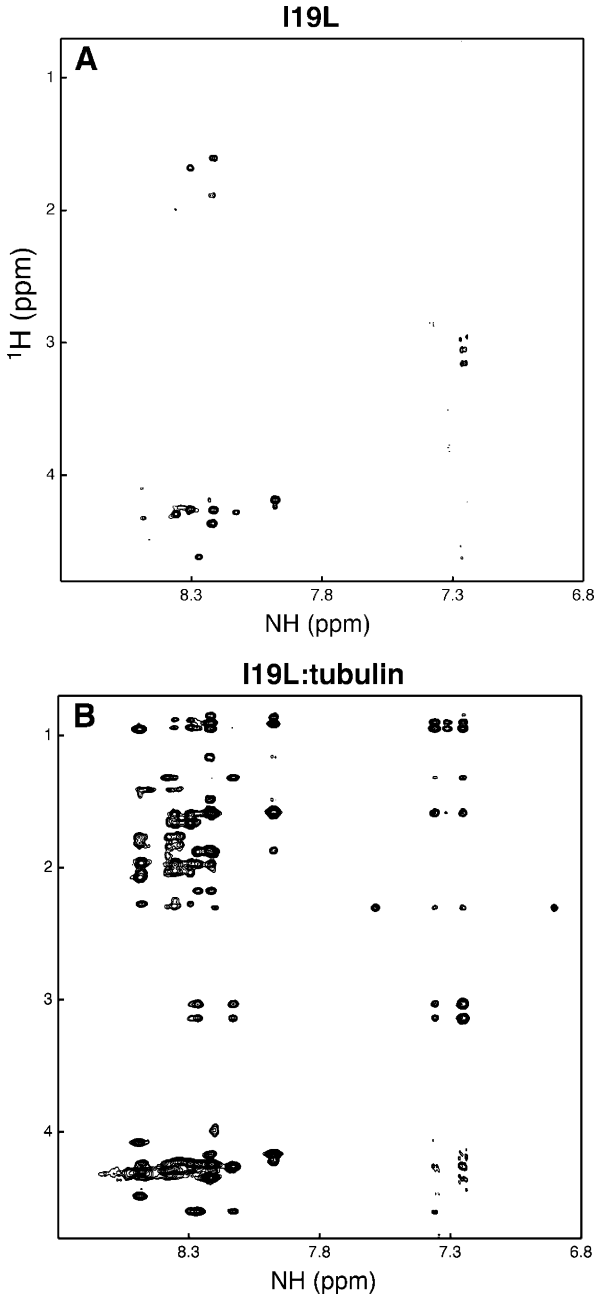

FIGURE 4: Tubulin-induced folding of I19L. (A) Region of the NOESY spectrum of the I19L peptide alone (0.6 mM) in H_2O/D_2O (90:10) at pH 6.8. (B) Same region of the TRNOESY spectrum of I19L in the presence of tubulin, with a ratio of 30:1 peptide/protein (0.6 mM peptide and 20 μM tubulin), in 50 mM phosphate buffer at pH 6.8. Spectra were recorded at 600 MHz and 294 K, with a mixing time of 200 ms.

(Figure 4). This clearly indicated that the intense negative NOEs are TRNOEs originating from the tubulin-bound conformation of I19L. Control TRNOESY experiments were also performed in the presence of BSA instead of tubulin to ascertain that negative NOEs were not originating from nonspecific peptide/protein interactions. The TRNOESY spectrum obtained in the latter conditions was similar to that of the free peptide, indicating that TRNOEs observed in the presence of tubulin are due to specific interactions of I19L with tubulin.

The analysis of these TRNOEs showed many medium- and long-range NOEs. For example, TRNOEs were observed between protons of residues Val-8 and Leu-22, Glu-10, and Phe-20 or Glu-12 and Ala-19, suggesting that I19L adopts a specific folding by the interaction with tubulin. Structure calculations of I19L bound to tubulin were performed with CNS 1.1 using 176 distance constraints derived from the TRNOESY spectrum. The structural statistics of the 10 best structures calculated are summarized in Table 1. No violation larger than 0.5 Å is observed in these structures. The structures display good covalent geometry, and all of the backbone Φ and Ψ dihedral angles are located in the allowed regions of the Ramachandran plot. The 10 best structures present a β-hairpin fold composed of two antiparallel β-strands (β1 and β2) comprising residues 8−14 and 17−22, respectively. A C+ β bulge (*46*) is observed at residues 11−12 (β1); these residues were pointed out by NMR spectroscopy and predicted by AGADIR to possess a helix-forming propensity (see above). The β-hairpin is rather well-defined with a mean pairwise root-mean-square deviation (rmsd) of 0.42 ± 0.13 and 1.25 ± 0.21 Å for the backbone and the heavy atoms, respectively. According to the mean pairwise rmsd, the second strand is however better defined than the first one (Table 1). The dispersion of the backbone observed at the turn and at the N- and C-terminal ends of the peptide (Figure 5B) reflects the flexibility of these regions. Hydrogen-bond calculation with MOLMOL (*38*) shows that the β-hairpin structure is stabilized by eight hydrogen bonds between backbone atoms of the two strands (Figure 5A). The hydrophobic interactions observed between residues Val-8 (β1) and Leu-22 (β2) and between Leu-11 (β1) and Ala-19 (β2) are also likely to participate in the stabilization of this structure. Finally, the presence of the bulge changes the usual distribution of side chains alternatively on each side of the β-sheet and brings Glu-10 and Lys-13 side chains close in space, thus allowing an ionic interaction between these residues (Figure 5A). Overall, these results show that the interaction of I19L with tubulin is a specific event that strongly induces the structure stabilization of this peptide, which would otherwise remain in a random coil conformation.

Table 1: Structural Statistics for the 10 Best Conformers Calculated for I19L

number of distance restraints	
intraresidue ($i - j = 0$)	80
sequential ($i - j = 1$)	46
medium range $2 \leq i - j \leq 4$	24
long range $i - j > 4$	26
total	176
number of distance violations >0.5 Å	0
rmsd values from idealized	
covalent geometry[a]	
bonds (Å)	0.0075 ± 0.0003
angles (deg)	0.826 ± 0.039
impropers (deg)	0.616 ± 0.058
Ramachandran plots (%)	
most favored regions	78.1
additionally allowed regions	21.9
mean pairwise rmsd values (Å)[b]	
all residues (6−24)	0.59 ± 0.19/1.40 ± 0.22
β-hairpin (8−22)	0.42 ± 0.13/1.25 ± 0.21
β1 strand (8−15)	0.32 ± 0.11/1.42 ± 0.28
β2 strand (17−22)	0.24 ± 0.10/0.77 ± 0.25

[a] rmsd values calculated using CNS. [b] rmsd values (backbone atoms/heavy atoms) calculated using MOLMOL.

Hydrophobic Residues of the I19L β2-Strand Participate in Its Interaction with Tubulin. We used STD−NMR

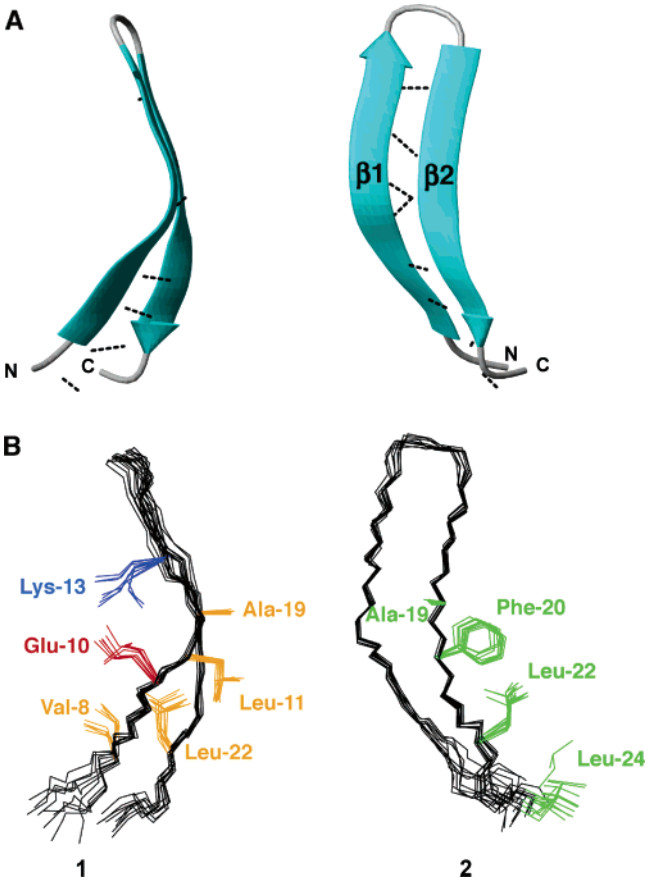

FIGURE 5: NMR structure of I19L in the interaction with tubulin. (A) Ribbon diagrams of the backbone atoms of the average structure of I19L, with hydrogen bonds between backbone atoms as dotted lines. (B) Superposition of the backbone atoms of the 10 best NMR structures of I19L. (1) Side chains of residues that stabilize the I19L folding are highlighted (red and blue, ionic interaction between E10 and K13; orange, hydrophobic interactions between V8 and L22 and between L11 and A19). (2) Side chains of residues of I19L in contact with tubulin derived from STD−NMR experiments are displayed in green.

spectroscopy (*22*), in the same experimental conditions as for the TRNOESY experiments, to identify which protons of I19L are in proximity to tubulin in the I19L/tubulin complex in solution. During the 1D STD−NMR experiments, the resonances of tubulin were saturated at 0 or 10 ppm, corresponding respectively to the resonance frequencies of protons of methyl groups and to the indole ring of tryptophan residues present in the protein. I19L, which is in fast exchange on the chemical-shift scale between free and bound forms, becomes saturated when bound to tubulin. Difference spectra recorded with and without protein saturation reveal protons of I19L in close contact with tubulin (Figure 6). They show that only a few resonances were affected by saturation of tubulin, and importantly, they were identical when tubulin was saturated either at 0 or 10 ppm. Thus, the spectra obtained with saturation of tubulin at 0 ppm are due to the interaction of I19L with tubulin and not to artifacts because of the irradiation of methyl protons of I19L. The accurate identification of protons of I19L in contact with tubulin was then achieved by means of 2D STD−TOCSY. These experiments show that the methyl group of Ala-19, the aromatic protons of Phe-20, and the side chains of Leu-22 and Leu-24 are in contact with tubulin. Interestingly, this series of hydrophobic residues is clustered on the β2-strand of I19L and points toward opposite directions: Ala-19 on one side and Phe-20, Leu-22, and Leu-24 on the other (Figure 5B).

I19L Docks α *Tubulin at the Longitudinal Tubulin Interdimer Interface*. To improve our understanding of I19L interaction with tubulin, we modeled it by molecular docking. A model of the I19L/tubulin complex was computed with FTDOCK, which evaluates the surface shape and the electrostatic complementarities of two molecules and docks them together as rigid bodies (*39*). Figure 7 displays the best docked position, in agreement with STD−NMR data, of I19L into the α-tubulin structure determined from the tubulin−colchicine/RB3−SLD crystal. According to this model and as observed for the N terminus of RB3 in the tubulin−colchicine/RB3−SLD crystal, I19L fits a pocket located on α tubulin at the interdimer interface between helix H10 and β-strand S9 and the I19L β-hairpin extends the tubulin intermediate β-sheet domain. The β2-strand of I19L faces tubulin and might establish hydrophobic interactions via residues identified by STD−NMR. Thus, Ala-19 may interact with residues of a tubulin bend formed by Ala-α247 and Leu-α248; Phe-20, Leu-22, and Leu-24 with residues of tubulin helix H10 (Val-α328 and Ile-α332) and β-strand S9 (Phe-α351 and Val-α353). The spatial organization of these hydrophobic interacting side chains pointing to opposite directions might hence "lock" the overall interaction with tubulin. In addition to these hydrophobic interactions, the side chain of residue Arg-14 located on the β1-strand of I19L might form an ionic interaction with tubulin residue Asp-α245 located at the surface of α-tubulin. It is worth noting that its orientation is also determined by the presence of the bulge. Finally, intermolecular hydrogen bonds could likely form between the amide protons of Leu-22 and Val-α353 and the carbonyl atoms of Phe-α351 and Phe-20, respectively, and the Nϵ of Arg-14 and the amide proton of Ala-α247.

DISCUSSION

Microtubules are filamentous intracellular structures involved in cell division, organization of intracellular structure, intracellular transport, as well as ciliary and flagellar motility. Because the functions of microtubules are so critical to the existence of eukaryotic cells, it is important to understand their regulation and to have molecules at one's disposal to modulate their assembly for therapeutic purposes. Stathmin family proteins share stathmin-like domains that have been shown to sequester tubulin and hence regulate microtubule dynamics *in vitro* and *in vivo*. We reported here the function of a novel series of conventional short peptides derived from stathmin-like domains that oppose tubulin assembly. These results enlighten the mechanism of tubulin sequestration by stathmin-like domains from which they derive and pave the way for the development of novel protein-based drugs or compounds aimed at interfering with tubulin polymerization.

Peptides Derived from the N-Terminal Cap of Stathmin-like Domains Function as Autonomous Tubulin Polymerization Inhibitors. A series of independent experiments suggested that the N-terminal part of SLDs was implicated in the inhibition of longitudinal tubulin−tubulin interaction (*7*, *18*, *19*, *21*, *47*). The present work extends these observations by showing that a minimal functional unit

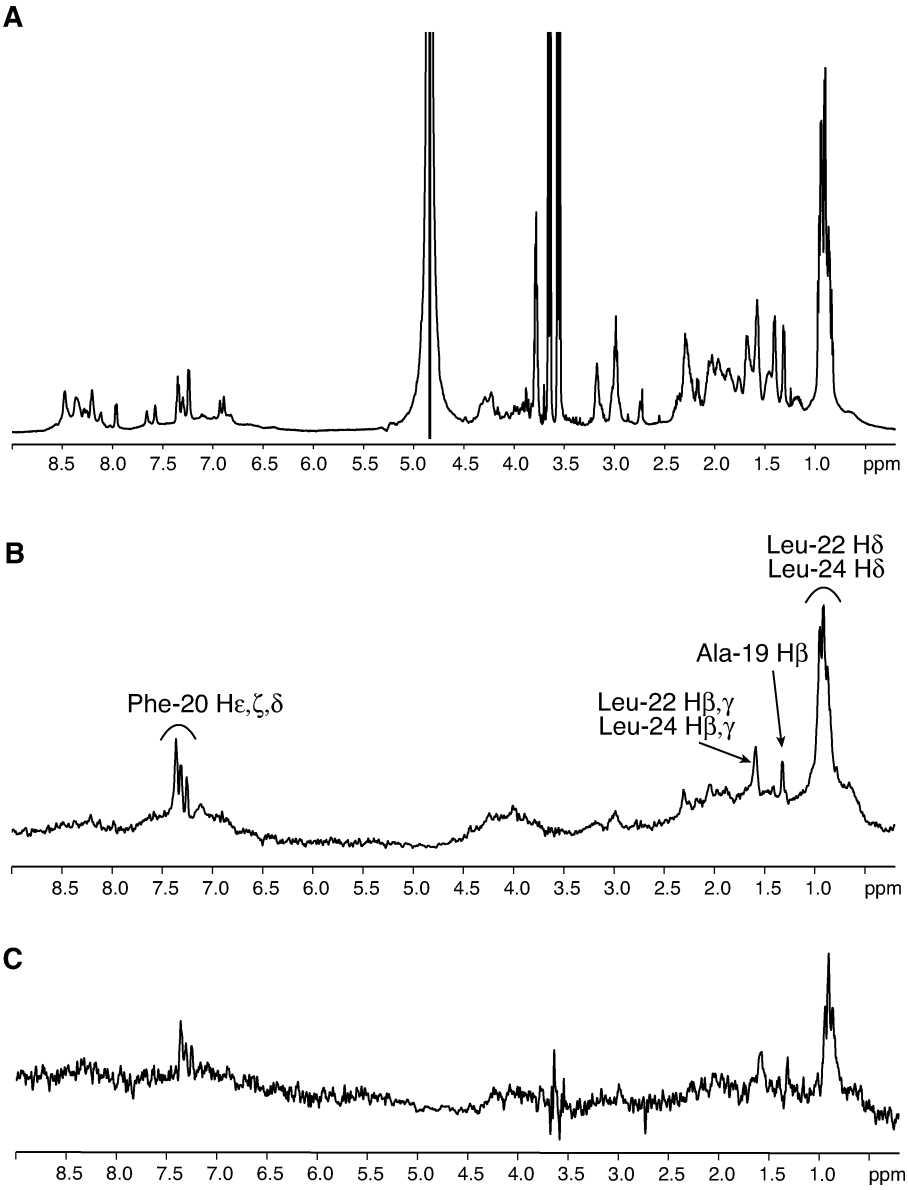

FIGURE 6: Series of hydrophobic residues from I19L interacts with tubulin. (A) One-dimensional ^{1}H NMR spectrum of I19L in the presence of tubulin. (B and C) One-dimensional STD−NMR spectra of I19L in the presence of tubulin with selective saturation of protein resonances at 0 and 10 ppm, respectively. Protons of I19L affected by the selective saturation of tubulin are labeled.

preventing tubulin association can be derived from a subdomain of the N-terminal part of SLDs. The results show that, to be fully effective, this unit must cover a short region (ca. 20 residues between amino acids 6−24) centered around the sequence that folded into a β-hairpin in the tubulin−colchicine/RB3−SLD crystal. In fact, IC_{50} dropped dramatically when peptides were designed to represent only the region homologous to the β-strand facing tubulin. Although the polymerization experiments do not allow a direct measurement of the binding, because the method does not distinguish between binding to tubulin and inhibition of polymerization, IC_{50} reflects apparent constants of the overall process and a decrease of IC_{50} most likely reflects a diminution of binding affinity of the peptide/tubulin interaction.

I19L Adopts an Original Structure Induced by the Interaction with Tubulin in Solution. I19L adopts a sophisticated β-hairpin structure in contact with tubulin in solution. The fact that such a short peptide possesses a well-organized structural element seems however uncommon, because only a few such examples have been reported. One of them concerns EGF-like subdomains in their thrombin-bound state, but in this case, an interstrand disulfide bridge appeared necessary to maintain the correct folding of the peptide (*48*). Another example was a 13-mer peptide that interacts with α bungarotoxin and behaves as a competitive inhibitor for its binding to the AChR (*49*). Interestingly, in this case, like in ours, the β-hairpin peptide forms an antiparallel β-sheet with its target protein that most likely contributes to the overall stability of the β-hairpin structure.

In Solution, I19L Structure in the Interaction with Tubulin Resembles That Observed in the SLD/Tubulin Crystal. The present NMR-resolved tubulin-induced folding of I19L in solution is close to that of the corresponding SLD region in the tubulin−colchicine/RB3−SLD crystal (*18*) (backbone rmsd of 1.55 Å), as well as that of the stathmin capping region within a stathmin−RB3 chimera in a crystal with tubulin−colchicine (backbone rmsd of 1.71 Å; B. Gigant and M. Knossow, personal data). A comparison of backbone dihedral angles of the NMR average structure of I19L with

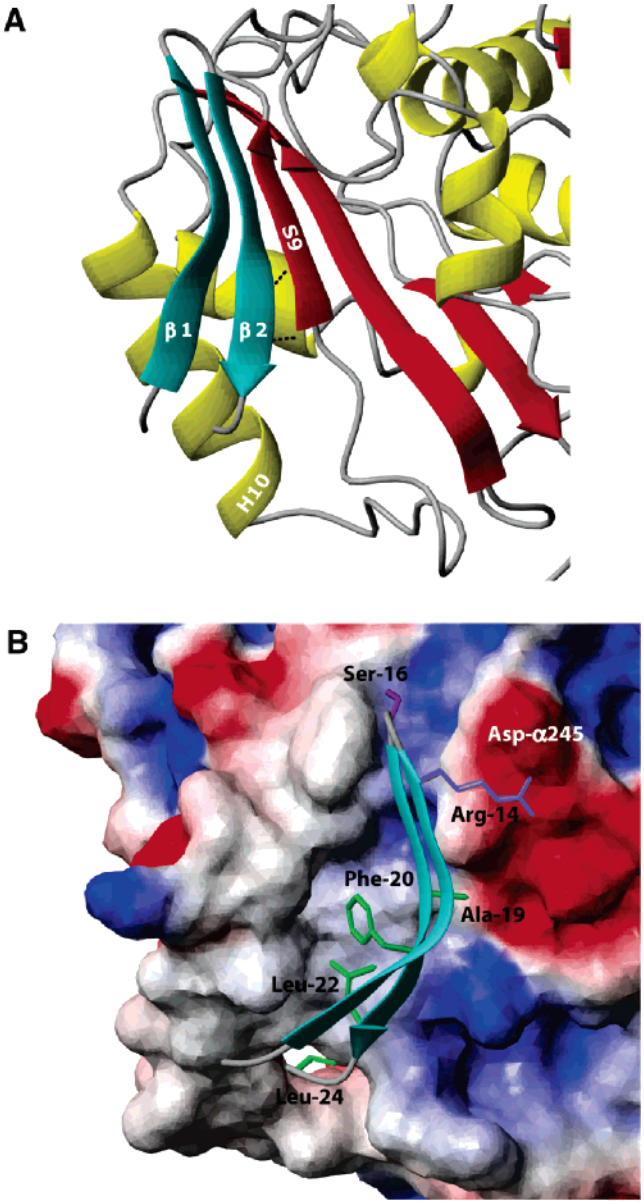

FIGURE 7: I19L likely extends the intermediate domain β-sheet of α-tubulin while docking into a hydrophobic pocket. (A) Ribbon representation of the I19L/tubulin complex obtained by docking calculations. I19L secondary structure elements are displayed in blue, and tubulin secondary structure elements are displayed in red and yellow (H10, helix 10; S9, strand 9). Dotted lines represent hydrogen bonds. (B) I19L docked over the electrostatic surface representation of tubulin from the X-ray crystal data of Ravelli et al. (*18*). Side chains of I19L residues in contact with tubulin (<5 Å) according to STD−NMR spectra are shown in green. The side chain of Arg-14 might engage in the ionic interaction with residue Asp-α245. The side chain of Ser-16 (phosphorylatable) points toward tubulin (negative charge is shown in red, positive in blue, and neutral in gray).

those of the corresponding region in tubulin−colchicine/RB3−SLD or tubulin−colchicine/stathmin−RB3 crystal structures shows however differences located at the N- and C-terminal ends of the peptide and around the bulge (residues 11−12). Differences at both termini originate from the usual flexibility of these regions in solution. Those around the bulge may arise from the better resolution of the NMR structure compared to crystals. Indeed, the electron-density maps of both crystal complexes are not well-defined around the β-hairpin N-terminal region, thus allowing us to super-

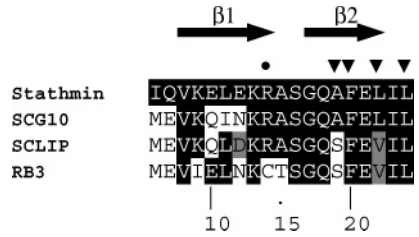

FIGURE 8: Sequence conservations and divergences within the I19L and β-hairpin region of the various stathmin family proteins. Sequence alignment of the corresponding sequences of the various members of the stathmin family from mammals showing identities (black boxed), similarities (gray), and divergences (white background) as compared to the stathmin I19L peptide. (▼) Amino acid residues identified by STD−NMR to interact with tubulin. (●) Arginine residue that likely engages in the ionic interaction with tubulin according to the I19L−tubulin complex model. β-strands revealed in I19L by NMR are indicated by arrows.

impose the crystal structures to NMR structures by rotations of crystal backbone dihedral angles while remaining in the electron-density envelope.

Altogether, the close similarity between the solution and the crystal structure indicates that the X-ray structure captured the general features of the interaction of the N-terminal cap with tubulin that actually exists in solution. It also indicates that the β-hairpin tubulin-induced folding of region 6−24 does not need this region to be linked and hence interact with the rest of the SLD molecule. Therefore, we were successful here in defining a minimal unit of the N-terminal capping region of SLDs essential for both folding and activity.

Conservation of Residues Involved in Structuring the β-Hairpin and Tubulin Interaction within the Stathmin Family. Sequence alignment of the N-terminal sequences corresponding to the β-hairpin within the various members of the stathmin family (Figure 8) reveals that the region corresponding to the second strand, the one interacting directly with tubulin, is much more conserved than the first one. Taking into account the amino acid residues identified as implicated in the interaction, we derived the following pattern to screen protein databases with the PATTERN package (*50*): Vxx[L/I]xKxxxGx[A/S]Fx[L/V]xL. Interestingly, only the stathmin family members were retrieved from mammalian sequences with this pattern, indicating that it represents a signature for the stathmin family. A closer look at sequence conservation in the framework of the structure reveals some of the molecular bases that may account for this conservation: the Val-8−Leu/Val-22 pair provides interstrand hydrophobic interactions; Leu-11 is nearly conserved (isoleucine in SCG10), whereas a hydrophobic partner at position 19 is conserved only in SCG10 (Ala-19). Importantly, three of the hydrophobic residues identified by STD−NMR experiments to interact with tubulin (Phe-20, Leu-22, and Leu-24) are conserved (valine substitutes Leu-22 in SCLIP and RB3). On the other hand, Ala-19 is present only in stathmin and SCG10 and is replaced by a serine residue in SCLIP and RB3, a variation that may account for the lower inhibitory activity of these peptides. Finally, from the I19L−tubulin docking model, it appears that Arg-14, which is changed for a cysteine residue in RB3, most likely makes an ionic interaction with tubulin and thus participates in increasing the binding affinity, which may explain its higher inhibition efficiency. Furthermore, among the other

conserved residues, the presence of a glycine residue seems mandatory at position 17, because, in the docking model, there is no room at position 17 for the presence of a side chain in the complex of the SLD N-terminal cap with tubulin. Altogether, it appears that many of the residues involved in structuring the I19L peptide in the interaction with tubulin are conserved within the stathmin family. The sequence divergences between stathmin family members account for the differences of the peptide−tubulin interaction reported, likely contributing to the individual biological specificities of SLDs in agreement with our previous biochemical studies on intact or chimeric SLDs (*3*, *17*, *21*, *51*). In this respect, M19L, derived from RB3, accumulates two unfavorable specific residue changes that may account for its lowest activity among the long peptides: the loss of the Leu-11−Ala-19 interstrand hydrophobic interaction and of the Ala-19 and Arg-14 interactions with tubulin; and a Leu22Val substitution which may weaken hydrophobic interaction with tubulin.

Influence of Ser-16 Phosphorylation on I19L Binding to Tubulin. Phosphorylation of peptide I19L on Ser-16 induces a reduction of its efficiency against tubulin polymerization (Figure 2), in agreement with a similar effect observed after phosphorylation of stathmin on the corresponding residue (*10*, *52*). Our data help us understand on a molecular basis the mechanism of this reduction. The docking model predicts that the side chain of serine 16 is oriented toward tubulin (Figure 7B). Thus, a first hypothesis for the reduction of inhibitory activity induced by phosphorylation is that the introduction of a bulky hydrophilic group would result in a steric hindrance that would weaken the affinity of I19L for tubulin and potentially further impede the formation of its tubulin-induced β-hairpin structure. In addition, the intramolecular ionic interaction between the phosphate group on serine 16 and the Arg-14 side chain might compete with the ionic interaction between Arg-14 and tubulin observed in the docking model.

Antimicrotubule Peptides Pave the Way for the Development of Novel Protein-Based Drugs or Compounds Aimed at Interfering with Tubulin Polymerization. Microtubules are key molecular targets for cancer therapy. To the best of our knowledge, this work is the first to report an antimicrotubule activity for short conventional synthetic peptides. Actually, tubulin polymerization is targeted by natural peptides or depsipeptides (one or more amide bonds replaced by ester bonds) isolated from a wide range of organisms that however contain unusual amino acids. Some of these, such as dolastatins or cryptophycins, are considered as potential anticancer drugs (review in ref *53*). A significant subset of these compounds (dolastatin 10, crytophycin 1, phomopsin A, and hemiasterlin) inhibits the binding of vinca alkaloids to tubulin in a noncompetitive manner and thus are the subject of intensive pharmacological research to find a common pharmacophore. The series of peptides evaluated in the present study may possess some advantages for a quick discovery of a pharmacophore of interest because their structures and functions although heterogeneous are not as disperse as for the above-mentioned (depsi)peptides.

In conclusion, we bring functional and structural evidences that short peptides derived from the N-terminal part of the stathmin-like domains of stathmin family proteins are autonomous inhibitors of tubulin polymerization. This work provides a rationale on a molecular basis for a better understanding of the common and specific functions of the N-terminal part of stathmin family proteins in capping tubulin and in interfering with microtubule assembly. It also represents a starting point to develop protein-based drugs or to design new lead compounds aimed at inhibiting tubulin polymerization notably in the context of cancer.

ACKNOWLEDGMENT

We thank Drs. Hervé Desvaux and Constantin Craescu for their help and fruitful discussions.

SUPPORTING INFORMATION AVAILABLE

A table containing proton chemical shifts of I19L in H_2O:D_2O (90:10) at pH 6.8 and 294 K. This material is available free of charge via the Internet at http://pubs.acs.org.

REFERENCES

1. Sobel, A., Boutterin, M. C., Beretta, L., Chneiweiss, H., Doye, V., and Peyro-Saint-Paul, H. (1989) Intracellular substrates for extracellular signaling: Characterization of a ubiquitous, neuron-enriched phosphoprotein (Stathmin). *J. Biol. Chem. 264*, 3765−3772.
2. Sobel, A. (1991) Stathmin: A relay phosphoprotein for multiple signal transduction? *Trends Biochem. Sci. 16*, 301−305.
3. Gavet, O., Ozon, S., Manceau, V., Lawler, S., Curmi, P., and Sobel, A. (1998) The stathmin phosphoprotein family. Intracellular localization and effects on the microtubule network, *J. Cell Sci. 111*, 3333−3346.
4. Holmfeldt, P., Larsson, N., Segerman, B., Howell, B., Morabito, J., Cassimeris, L., and Gullberg, M. (2001) The catastrophe-promoting activity of ectopic Op18/stathmin is required for disruption of mitotic spindles but not interphase microtubules, *Mol. Biol. Cell 12*, 73−83.
5. Jourdain, L., Curmi, P., Sobel, A., Pantaloni, D., and Carlier, M. F. (1997) Stathmin: A tubulin-sequestering protein which forms a ternary T2S complex with two tubulin molecules, *Biochemistry 36*, 10817−10821.
6. Curmi, P. A., Andersen, S. S. L., Lachkar, S., Gavet, O., Karsenti, E., Knossow, M., and Sobel, A. (1997) The stathmin/tubulin interaction *in vitro*, *J. Biol. Chem. 272*, 25029−25036.
7. Steinmetz, M. O., Kammerer, R. A., Jahnke, W., Goldie, K. N., Lustig, A., and van Oostrum, J. (2000) Op18/stathmin caps a kinked protofilament-like tubulin tetramer, *EMBO J. 19*, 572−580.
8. Gigant, B., Curmi, P. A., Martin-Barbey, C., Charbaut, E., Lachkar, S., Lebeau, L., Siavoshian, S., Sobel, A., and Knossow, M. (2000) The 4 Å X-ray structure of a tubulin:stathmin-like domain complex, *Cell 102*, 809−816.
9. Redeker, V., Lachkar, S., Siavoshian, S., Charbaut, E., Rossier, J., Sobel, A., and Curmi, P. (2000) Probing the native structure of stathmin and its interaction domains with tubulin, *J. Biol. Chem. 275*, 6841−6849.
10. Amayed, P., Pantaloni, D., and Carlier, M. F. (2002) The effect of stathmin phosphorylation on microtubule assembly depends on tubulin critical concentration, *J. Biol. Chem. 277*, 22718−22724.
11. Belmont, L. D., and Mitchison, T. J. (1996) Identification of a protein that interacts with tubulin dimers and increases the catastrophe rate of microtubules, *Cell 84*, 623−631.
12. Larsson, N., Segerman, B., Howell, B., Fridell, K., Cassimeris, L., and Gullberg, M. (1999) Op18/stathmin mediates multiple region-specific tubulin and microtubule-regulating activities, *J. Cell Biol. 146*, 1289−1302.
13. Ozon, S., Maucuer, A., and Sobel, A. (1997) The stathmin family: Molecular and biological characterization of novel mammalian proteins expressed in the nervous system, *Eur. J. Biochem. 248*, 794−806.
14. Ozon, S., Byk, T., and Sobel, A. (1998) SCLIP: A novel SCG10-like protein of the stathmin family expressed in the nervous system, *J. Neurochem. 70*, 2386−2396.
15. Stein, R., Mori, N., Matthews, K., Lo, L. C., and Anderson, D. J. (1988) The NGF-inducible SCG10 mRNA encodes a novel membrane-bound protein present in growth cones and abundant in developing neurons, *Neuron 1*, 463−476.

16. Maucuer, A., Moreau, J., Mechali, M., and Sobel, A. (1993) The stathmin gene family: Phylogenetic conservation and developmental regulation in *Xenopus*, *J. Biol. Chem. 268*, 16420−16429.
17. Charbaut, E., Curmi, P. A., Ozon, S., Lachkar, S., Redeker, V., and Sobel, A. (2001) Stathmin family proteins display specific molecular and tubulin binding properties, *J. Biol. Chem. 276*, 16146−16154.
18. Ravelli, R. B. G., Gigant, B., Curmi, P. A., Jourdain, I., Lachkar, S., Sobel, A., and Knossow, M. (2004) Insight into tubulin regulation from a complex with colchicine and a stathmin-like domain, *Nature 428*, 198−202.
19. Muller, D. R., Schindler, P., Towbin, H., Wirth, U., Voshol, H., Hoving, S., and Steinmetz, M. O. (2001) Isotope-tagged cross-linking reagents. A new tool in mass spectrometric protein interaction analysis, *Anal. Chem. 73*, 1927−1934.
20. Nogales, E., Whittaker, M., Milligan, R. A., and Downing, K. H. (1999) High-resolution model of the microtubule, *Cell 96*, 79−88.
21. Jourdain, I., Lachkar, S., Charbaut, E., Gigant, B., Knossow, M., Sobel, A., and Curmi, P. A. (2004) A synergistic relationship between three regions of Stathmin family proteins is required for the formation of a stable complex with tubulin, *Biochem. J. 378*, 877−888.
22. Mayer, M., and Meyer, B. (1999) Characterization of ligand binding by saturation transfer difference NMR spectra, *Angew. Chem. Int. Ed. 35*, 1784−1788.
23. Shelanski, M. L., Gaskin, F., and Cantor, C. R. (1973) Microtubule assembly in the absence of added nucleotides, *Proc. Natl. Acad. Sci. U.S.A. 70*, 765−768.
24. Weingarten, M. D., Lockwood, A. H., Hwo, S. Y., and Kirschner, M. W. (1975) A protein factor essential for microtubule assembly, *Proc. Natl. Acad. Sci. U.S.A. 72*, 1858−1862.
25. Detrich, H. W., III, and Williams, R. C. (1978) Reversible dissociation of the α β dimer of tubulin from bovine brain, *Biochemistry 17*, 3900−3917.
26. Rance, M., Sorensen, O. W., Bodenhausen, G., Wagner, G., Ernst, R. R., and Wuthrich, K. (1983) Improved spectral resolution in cosy ^{1}H NMR spectra of proteins via double quantum filtering, *Biochem. Biophys. Res. Commun. 117*, 479−485.
27. Braunschweiler, L., and Ernst, R. R. (1983) Coherence transfer by isotropic mixing: Application to proton correlation spectroscopy, *J. Magn. Reson. 53*.
28. Kumar, A., Ernst, R. R., and Wüthrich, K. (1980) A two-dimensional nuclear Overhauser enhancement (2D NOE) experiment for the elucidation of complete proton−proton cross-relaxation networks in biological macromolecules, *Biochem. Biophys. Res. Commun. 95*, 1−6.
29. Bax, A., and Davies, D. G. (1985) Practical aspects of two-dimensional transverse NOE spectroscopy, *J. Magn. Reson. 63*, 207−213.
30. Bax, A., and Davies, D. G. (1985) MLEV-17-based two-dimensional homonuculear magnetization transfer spectroscopy, *J. Magn. Reson. 65*, 355−360.
31. Clore, G. M., and Gronenborn, A. M. (1982) Theory and applications of the transferred nuclear Overhauser effect to the study of the conformations of small ligands bound to proteins, *J. Magn. Reson. 48*, 402−417.
32. Clore, G. M., and Gronenborn, A. M. (1983) Theory of the time dependent transferred nuclear Overhauser effect: Application to the structural analysis of ligand−protein complexes in solution, *J. Magn. Reson. 53*, 423−442.
33. Piotto, M., Saudek, V., and Sklenar, V. (1992) Gradient-tailored excitation for single-quantum NMR spectroscopy of aqueous solutions, *J. Biomol. NMR 2*, 661−665.
34. Johnson, B. A., and Blevins, R. (1994) A NMRView: A computer program for the visualization and analysis of NMR data, *J. Biomol. NMR 4*, 603−614.
35. Baleja, J., Moult, J., and Sykes, B. D. (1990) Distance measurement and structure refinement with NOE data, *J. Magn. Reson. 87*, 375−384.
36. Brünger, A. T., Adams, P. D., Clore, G. M., DeLano, W. L., Gros, P., Grosse-Kunstleve, R. W., Jiang, J. S., Kuszewski, J., Nilges, M., P. N. S., et al. (1998) Crystallography and NMR system: A new software suite for macromolecular structure determination, *Acta Crystallogr., Sect. D: Biol. Crystallogr. 54*, 905−921.
37. Laskowski, R. A., MacArthur, M. W., Moss, D. A., and Thornton, J. M. (1993) PROCHECK: A program to check the stereochemical quality of protein structures, *J. Appl. Crystallogr. 26*, 283−291.
38. Koradi, R., Billeter, M., and Wüthrich, K. (1996) MOLMOL: A program for display and analysis of macromolecular structures, *J. Mol. Graphics 14*, 51−55.
39. Gabb, H. A., Jackson, R. M., and Sternberg, M. J. (1997) Modelling protein docking using shape complementarity, electrostatics, and biochemical information, *J. Mol. Biol. 272*, 106−120.
40. Beretta, L., Dobransky, T., and Sobel, A. (1993) Multiple phosphorylation of stathmin: Identification of four sites phosphorylated in intact cells, and *in vitro* by cyclic-AMP dependent protein kinase and p34cdc2, *J. Biol. Chem. 268*, 20076−20084.
41. le Gouvello, S., Manceau, V., and Sobel, A. (1998) Serine 16 of stathmin as a cytosolic target for Ca^{2+}/calmodulin-dependent kinase II after CD2 triggering of human T lymphocytes, *J. Immunol. 161*, 1113−1122.
42. Melander Gradin, H., Marklund, U., Larsson, N., Chatila, T. A., and Gullberg, M. (1997) Regulation of microtubule dynamics by Ca^{2+}/calmodulin-dependent kinase IV/Gr-dependent phosphorylation of oncoprotein 18, *Mol. Cell. Biol. 17*, 3459−3467.
43. Wittmann, T., Bokoch, G. M., and Waterman-Storer, C. M. (2004) Regulation of microtubule destabilizing activity of Op18/stathmin downstream of Rac1, *J. Biol. Chem. 279*, 6196−6203.
44. Wüthrich, K. (1986) *NMR of Proteins and Nucleic Acids*, John Wiley and Sons, New York.
45. Wishart, D. S., Bigam, C. G., Holm, A., Hodges, R. S., and Sykes, B. D. (1995) ^{1}H, ^{13}C, and ^{15}N random coil NMR chemical shifts of the common amino acids. I. Investigations of nearest-neighbor effects, *J. Biomol. NMR 5*, 67−81.
46. Chan, A. W., Hutchinson, E. G., Harris, D., and Thornton, J. M. (1993) Identification, classification, and analysis of β-bulges in proteins, *Protein Sci. 2*, 1574−1590.
47. Segerman, B., Holmfeldt, P., Morabito, J., Cassimeris, L., and Gullberg, M. (2003) Autonomous and phosphorylation-responsive microtubule-regulating activities of the N-terminus of Op18/stathmin, *J Cell Sci. 116*, 197−205.
48. Hrabal, R., Komives, E. A., and Ni, F. (1996) Structural resiliency of an EGF-like subdomain bound to its target protein, thrombin, *Protein Sci. 5*, 195−203.
49. Scherf, T., Kasher, R., Balass, M., Fridkin, M., Fuchs, S., and Katchalski-Katzir, E. (2001) A β-hairpin structure in a 13-mer peptide that binds α-bungarotoxin with high affinity and neutralizes its toxicity, *Proc. Natl. Acad. Sci. U.S.A. 98*, 6629−6634.
50. Cockwell, K. Y., and Giles, I. G. (1989) Software tools for motif and pattern scanning: Program descriptions including a universal sequence reading algorithm, *Comput. Appl. Biosci. 5*, 227−232.
51. Ozon, S., El Mestikawy, S., and Sobel, A. (1999) Differential, regional, and cellular expression of the stathmin family transcripts in the adult rat brain, *J. Neurosci. Res. 56*, 553−564.
52. Steinmetz, M. O., Jahnke, W., Towbin, H., Garcia-Echeverria, C., Voshol, H., Muller, D., and van Oostrum, J. (2001) Phosphorylation disrupts the central helix in Op18/stathmin and suppresses binding to tubulin, *EMBO Rep. 2*, 505−510.
53. Hamel, E., and Covell, D. G. (2002) Antimitotic peptides and depsipeptides, *Curr. Med. Chem. 2*, 19−53.
54. Koppel, J., Boutterin, M. C., Doye, V., Peyro-Saint-Paul, H., and Sobel, A. (1990) Developmental tissue expression and phylogenetic conservation of stathmin, a phosphoprotein associated with cell regulations, *J. Biol. Chem. 265*, 3703−3707.

BI0512492